Mixed-valence states formation in conformationally flexible metal-free 5,10,15,20-tetraferrocenylporphyrin and 5,10-bisferrocenyl-15,20-bisphenylporphyrin†

Victor N. Nemykin,*[a] Christopher D. Barrett,[a] Ryan G. Hadt,[a] Roman I. Subbotin,[a] Alexander Y. Maximov,[a] Ernst V. Polshin[b] and Alexey Y. Koposov[a]

Received 9th March 2007, Accepted 11th May 2007
First published as an Advance Article on the web 4th June 2007
DOI: 10.1039/b703581k

Metal-free 5,10,15,20-tetraferrocenylporphyrin and 5,10-bisferrocenyl-15,20-bisphenylporphyrin have been prepared and characterized by UV-Vis, MCD, ^{1}H, ^{13}C, and variable-temperature NMR, APCI- and ESI-MS, and Mössbauer spectroscopy, while their redox properties were investigated using electrochemical (cyclic voltammetry and differential pulse voltammetry), spectroelectrochemical, and chemical oxidation approaches. The electronic structure calculations at Density Functional Theory level reveal that both compounds adopt saddle conformations and the HOMOs in both complexes are predominantly metal-centered, while the LUMOs predominantly consist of porphyrin π* orbitals. In spite of the rotational freedom of ferrocenyl substituents at room temperature, both metal-free 5,10,15,20-tetraferrocenylporphyrin and 5,10-bisferrocenyl-15,20-bisphenylporphyrin are able to form mixed-valence states upon the successive ferrocene-based two- and one-electron oxidations, respectively, as confirmed by UV-Vis, MCD, Mössbauer, electro-, and spectroelectrochemical methods, and thus, the earlier suggested (Boyd *et al. Chem. Commun.*, 1999, 637) requirements for the formation of mixed-valence states in ferrocene-containing porphyrins should be revised.

Introduction

One of the most challenging problems in the preparation of nanoscale materials useful as molecular electronic devices is the synthesis of well-defined chemical systems with electronically coupled remote sites. In this respect, the formation of mixed-valence states in polynuclear transition-metal and, specifically, ferrocene-containing complexes is one of the most intriguing phenomena. Since the discovery of mixed-valence properties in bis(ferrocenyl) complexes, the chemistry of poly(metallocenes) with metal–metal coupling has resulted in a tremendous variety of remarkable structures interesting both from the fundamental nature of interaction between the metal centers (*i.e.* multiredox processes, magnetic coupling, and unpaired electron density migration) and practical points of view (*i.e.* opto-electronic materials for application in high-speed photonic or high-density memory devices).[1] To date, however, examples of poly(ferrocenes) exhibiting long-range (~10 Å) metal–metal coupling are extremely rare. Recently, two independent groups have reported a rare example of octa-β-alkyl-5,15-bis(ferrocenyl)porphyrins, which showed a long-range metal–metal coupling between two ferrocenyl substituents.[2] Both research teams have reasonably suggested that the probable reason for the observed metal–metal interaction is due to restricted conformational flexibility of ferrocene groups because in the case of 5,15-diferrocenyl-10,20-di-*p*-tolylporphyrin, in which ferrocenyl groups are conformationally flexible, it was claimed that no metal–metal coupling had been observed. In this paper, we report the preparation and redox properties of 5,10,15,20-tetraferrocenylporphyrin ($TFcPH_2$, Fig. 1) and 5,10-bisferrocenyl-15,20-bisphenylporphyrin (*cis*-$Fc_2Ph_2PH_2$, Fig. 1), which, despite rotational flexibility of ferrocene substituents, display long-range metal–metal coupling, suggesting that the conformational rigidity is not the only factor controlling the formation of mixed-valence states in ferrocenyl-containing porphyrins.

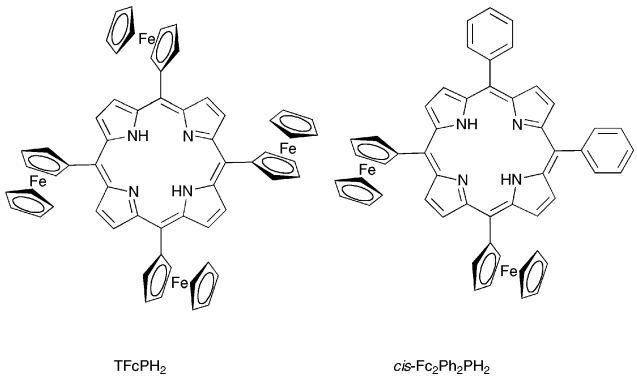

$TFcPH_2$ *cis*-$Fc_2Ph_2PH_2$

Fig. 1

Results and discussion

$TFcPH_2$ was prepared by classical condensation between ferrocene carbaldehyde and pyrrole as described previously,[3] while

[a]*Department of Chemistry and Biochemistry, University of Minnesota Duluth, 1039 University Drive, Duluth, MN, 55812, USA. E-mail: vnemykin@d.umn.edu; Fax: +1-218-726-7394; Tel: +1-218-726-6729*
[b]*Institute of Metal Physics, 28 Vernadsky Ave., Kiev, 01034, Ukraine*

† Electronic supplementary information (ESI) available: Variable-temperature NMR spectra of $TFcPH_2$, COSY NMR spectrum of *cis*-$Fc_2Ph_2PH_2$ and DFT predicted spin densities and quadrupole splittings in TFcPZn and $[TFcPZn]^{2+}$. See DOI: 10.1039/b703581k

cis-$Fc_2Ph_2PH_2$ was isolated from the reaction mixture in the statistical cross-condensation between ferrocene carbaldehyde, benzaldehyde, and pyrrole as described in the Experimental section.

The UV-Vis and MCD spectra of $TFcPH_2$ and *cis*-$Fc_2Ph_2PH_2$ (Fig. 2) confirm the aromatic macrocyclic nature of both complexes and reflect their molecular symmetries.[4] The UV-Vis spectrum of $TFcPH_2$ consists of an intense Soret band at 433 nm with a prominent shoulder at *ca*. 480 nm and, characteristic for metal-free porphyrins, two Q-bands observed at 664 and 728 nm. Compared to the well-known metal-free *meso*-tetraphenylporphyrin ($TPPH_2$) all bands in the UV-Vis spectrum of $TFcPH_2$ are shifted to low-energy positions, reflecting a greater electron-donating ability of ferrocenyl substituents in comparison to the phenyl ones. In agreement with the UV-Vis spectrum, the Soret band of $TFcPH_2$ is represented in the MCD spectrum by a Faraday pseudo *A*-term centered at 435 nm, while the shoulder observed at *ca*. 480 nm in the UV-Vis spectrum is represented by a weaker Faraday pseudo *A*-term centered at *ca*. 500 nm (Fig. 2). On the other hand, Q-bands in the MCD spectrum of $TFcPH_2$ are represented by a negative Faraday *B*-term observed at 727 nm and a positive Faraday *B*-term located at 669 nm. The UV-Vis spectrum of *cis*-$Fc_2Ph_2PH_2$ consists of an intense Soret band observed at 426 nm and two Q-bands observed at 616 and 692 nm (Fig. 2). Again, all these bands are blue-shifted in comparison to those in $TFcPH_2$ complex, confirming weaker electron-donating properties of the phenyl substituents in comparison to the ferrocenyl substituents. In analogy with $TFcPH_2$, the Soret band of *cis*-$Fc_2Ph_2PH_2$ is represented in the MCD spectrum by a Faraday pseudo *A*-term centered at 429 nm, while Q-bands are represented by a negative Faraday *B*-term observed at 650 nm and a positive Faraday *B*-term located at 622 nm.

The ^1H NMR spectrum of $TFcPH_2$ is similar to that reported earlier[3a] and consists of singlets corresponding to the pyrrolic β-protons, unsubstituted cyclopentadienyl ring, and inner NH protons, along with two triplets corresponding to the substituted cyclopentadienyl rings (Fig. 3). This simple picture becomes more complicated in the case of *cis*-$Fc_2Ph_2PH_2$. Indeed, lowering of the effective symmetry of this complex in comparison to that in $TFcPH_2$, results in four non-equivalent signals of β-pyrrolic protons in the ^1H NMR spectrum (Fig. 3). As expected, two resonance signals are singlets, while the other two are correlating doublets. In agreement with UV-Vis spectra of $TFcPH_2$ and *cis*-$Fc_2Ph_2PH_2$, protons of the ferrocene substituents in *cis*-$Fc_2Ph_2PH_2$ are slightly (~0.1 ppm) shifted downfield in comparison to those in $TFcPH_2$, pointing out the stronger electron-donating properties of ferrocene groups. Signals of inner NH protons in *cis*-$Fc_2Ph_2PH_2$ (−1.83 ppm) reflect a stronger shielding current created by the π-system inside of the porphyrin cavity in comparison to that in $TFcPH_2$, for which the resonance signal for NH protons was observed at −0.49 ppm.

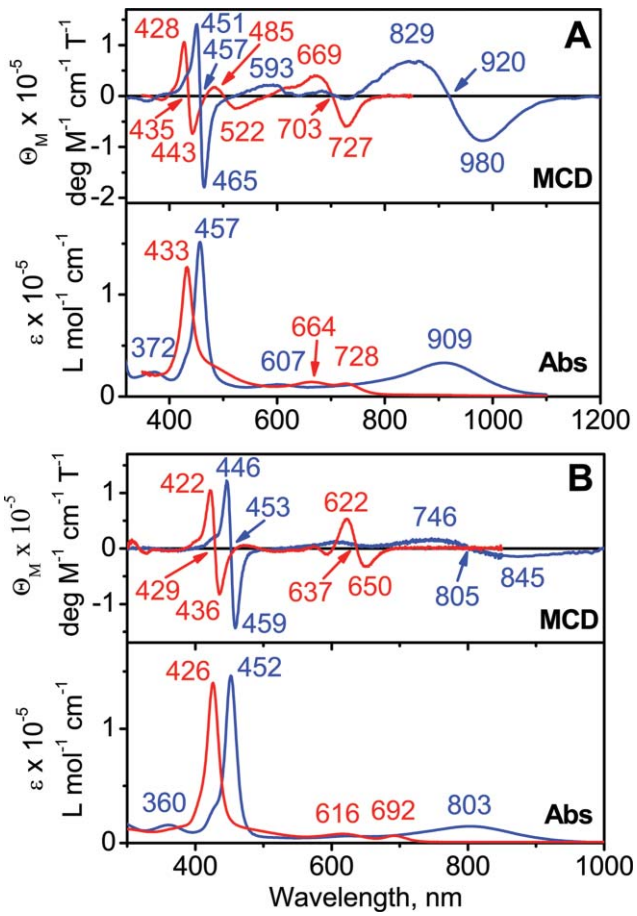

Fig. 2 UV-Vis and MCD spectra of neutral (red) and mixed-valence (blue) states of $TFcPH_2$ (A) and *cis*-$Fc_2Ph_2PH_2$ (B) in chloroform.

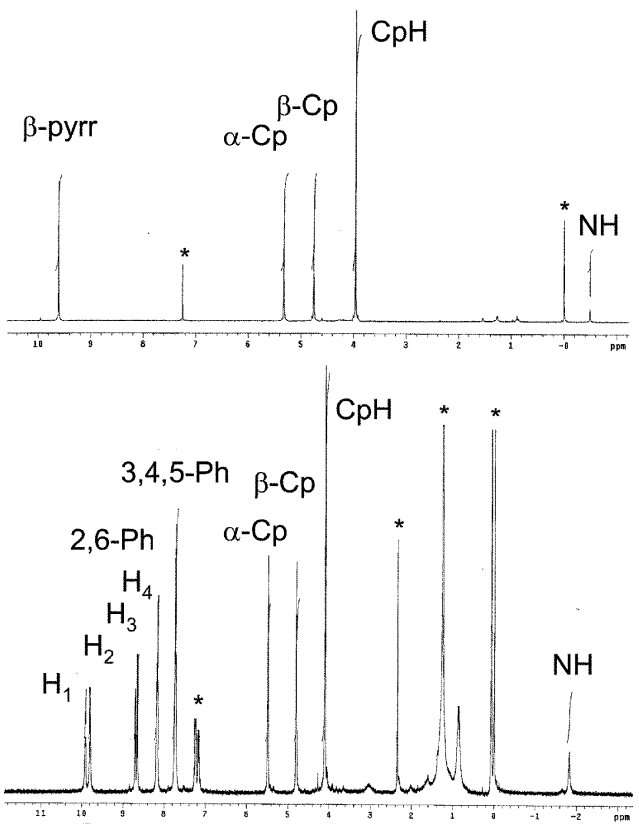

Fig. 3 Room-temperature ^1H NMR spectra of $TFcPH_2$ (top; solvent–$CDCl_3$) and *cis*-$Fc_2Ph_2PH_2$ (bottom; solvent–toluene-d_8). Solvent peaks are labeled with an asterisk.

An absence of substituents located at the β-positions of the pyrrole rings in $TFcPH_2$ and *cis*-$Fc_2Ph_2PH_2$ allows free rotation of ferrocene substituents around the C(*meso*)–C(Fc) bond at room temperature as it has been confirmed by variable-temperature NMR experiments. In the case of $TFcPH_2$, variable-temperature NMR experiments in THF reveal similar, but not identical, tendencies to those observed earlier for a TFcPZn complex.[3b] The signals of ferrocenyl substituents as well as inner NH protons became broader as temperature decreased (ESI†). The resonance signals of β-pyrrolic protons, however, undergo two distinct processes (ESI†). First, the initial singlet of β-pyrrolic protons splits into two relatively narrow components between 223 and 213 K. The coalescence temperature of this process is similar to that observed in the case of the TFcPZn complex,[3b] and thus, the first dynamic process was assigned to the elimination of rotational freedom of ferrocene substituents in $TFcPH_2$. Standard analysis of the first dynamic process[5] allows us to estimate a rotational barrier of ferrocene substituents in $TFcPH_2$ of ~10.4 kcal mol^{-1}. Further lowering of temperature down to 183 K results in collapse of the two β-pyrrolic proton signals observed between 223 and 183 K into one broad peak centered at *ca.* 9.52 ppm. This broad peak again splits into two very broad signals at temperatures lower than 183 K (ESI†). Since this process was not observed in the case of the TFcPZn complex, we attributed the second dynamic process to "freezing" of individual NH tautomers, similar to the well-known processes observed in symmetric and low-symmetry metal-free porphyrins.[6,7] The solvent freezing temperature does not allow resolution of observed broad signals into four individual bands as would be expected depending on the position of ferrocene substituents with respect to β-pyrrolic protons in $TFcPH_2$. The free enthalpy of activation of ~7.9 kcal mol^{-1}, however, was estimated for this process on the basis of coalescence temperature and positions of the broad peaks.[5]

The situation becomes more complicated in the case of *cis*-$Fc_2Ph_2PH_2$ (Fig. 4 and 5) and will be discussed in detail along with the variable-temperature NMR spectra of mono- and tri(ferrocenyl)-substituted porphyrins in a separate paper, while only a qualitative picture is discussed below. First of all, it should be noted that two simultaneous processes are expected in variable-temperature NMR spectra of this complex. First, in analogy with several metal-free low-symmetry porphyrins investigated earlier,[6] NH protons in *cis*-$Fc_2Ph_2PH_2$ can occupy three non-equivalent positions resulting in the formation of two possible tautomers at low temperature as presented in Fig. 6. DFT calculations on both tautomers suggest that tautomer **A** is only 0.02 kcal mol^{-1} lower in energy as compared to tautomer **B**, and thus, both of them should be observed in the variable-temperature NMR experiment.

Taking into consideration equivalent positions for NH protons in tautomer **A**, three NH signals are expected in the low-temperature NMR spectrum of *cis*-$Fc_2Ph_2PH_2$. Second, freezing rotation of ferrocenyl substituents at low temperature should affect the resonance position of β-pyrrolic protons in rings 1, 2, and 3 (Fig. 6), similarly to that observed in the case of $TFcPH_2$ and TFcPZn[3b] complexes.

The presence of two possible NH tautomeric forms can be clearly seen even from room-temperature ^1H NMR COSY experiments on *cis*-$Fc_2Ph_2PH_2$ in which weak correlation between NH and all β-pyrrolic protons was observed (ESI†) and was further confirmed by variable-temperature NMR data. Indeed,

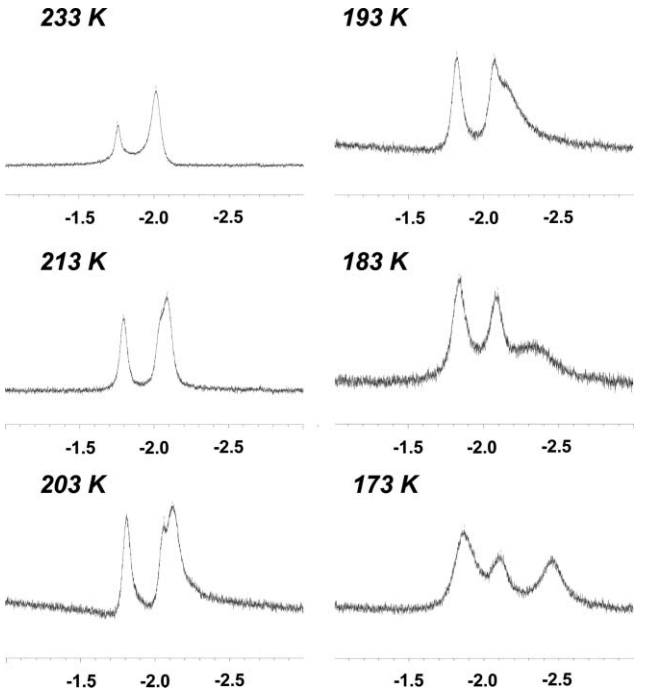

Fig. 4 Variable-temperature ^1H NMR spectra of *cis*-$Fc_2Ph_2PH_2$ in NH protons region in THF-d_8.

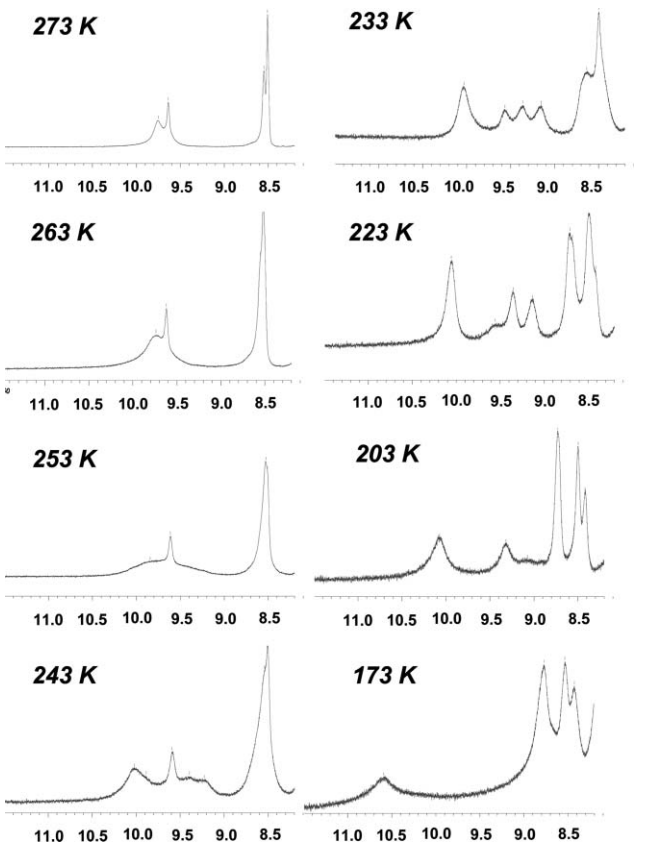

Fig. 5 Variable-temperature ^1H NMR spectra of *cis*-$Fc_2Ph_2PH_2$ in β-pyrrolic protons region in THF-d_8.

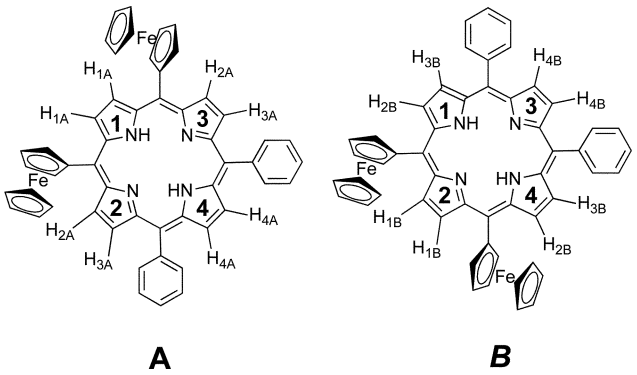

Fig. 6 Possible NH tautomers of *cis*-$Fc_2Ph_2PH_2$.

the lowering of temperature from 298 to 233 K results in the formation of two NH peaks at ~ −1.8 and −2.0 ppm with an integral ratio of 1 : 2 (Fig. 4). Further decrease of temperature leads to collapse of the major peak into two non-equivalent components confirming equilibrium between tautomers **A** and **B** (Fig. 6). An analysis of integral intensities suggests the presence of two-thirds of tautomer **A** and one-third of tautomer **B** at the low-temperature limit. Next, taking into consideration the larger size of ferrocene substituents in comparison to the phenyl ones, it is expected that β-pyrrolic protons H_{1A} and H_{1B} will be affected first in the variable-temperature NMR experiment followed by protons H_{1A} and H_{2B}, H_{3A} and H_{3B}, and finally H_{4A} and H_{4B} (Fig. 6). The qualitative observations are in excellent agreement with this prediction (Fig. 5). For instance, even a ten degree decrease in temperature leads to the collapse of the singlet belonging to H_{1A} and H_{1B} protons. Further decrease in temperature results in transformation of the peak corresponding to H_{2A} and H_{2B} protons into three clear components observed at 233 K. These components completely disappear at the low-temperature limit. Finally, the peak belonging to H_{4A} and H_{4B} protons splits into two components at low temperature confirming the presence of tautomers **A** and **B** similar to those observed in the case of metal-free tetraphenylporphyrin.[7]

APCI mass spectra of $TFcPH_2$ and *cis*-$Fc_2Ph_2PH_2$ are presented in Fig. 7 and almost exclusively consist of protonated molecular ions. As has been shown recently, collision-induced dissociation can provide valuable information on the stability of metal–ligand bonds in inorganic and organometallic compounds,[8] and thus, $TFcPH_2$ and *cis*-$Fc_2Ph_2PH_2$ complexes were investigated using APCI-MS/MS approach. The data presented in Fig. 8 and 9 reveal similar collision-induced fragmentation patterns for $TFcPH_2$ and *cis*-$Fc_2Ph_2PH_2$. In the case of $TFcPH_2$, the initially protonated molecular ion first eliminates an unsubstituted cyclopentadienyl ligand with the formation of a $[M–Cp–H]^+$ ion (Fig. 8). Further increase of collision energy leads to the dissociation of cyclopentadienyl- and ferrocene-fragments with the formation of $[M–Cp]^+$, $[M–2Cp]^+$, $[M–Fc–Cp–H]^+$, and $[M–Fc–2Cp]^+$ ions as the major fragments, while the nature of the $[M-59]^+$ ion, which appears at high collision energies, will be confirmed in the future on the basis of high-resolution experiments.

A similar $[M-59]^+$ ion has also been observed in the case of the high-energy limit in collision-induced dissociation of *cis*-$Fc_2Ph_2PH_2$, along with $[M–Cp]^+$, $[M–2Cp]^+$, $[M–Fc]^+$, $[M–Fc–Cp–H]^+$, and $[M–Fc–Cp–Ph]^+$ ions (Fig. 9). Overall, collision-induced dissociation of $TFcPH_2$ and *cis*-$Fc_2Ph_2PH_2$ leads to the fragmentation of the cyclopentadienyl ligands and *meso*-substituents, while the porphyrin core remains intact with an excellent agreement to previously discussed fragmentation patterns on porphyrin compounds.[9]

The electronic structures of $TFcPH_2$ and both possible tautomers of *cis*-$Fc_2Ph_2PH_2$ were calculated at the DFT level. The optimized molecular structures are presented in Fig. 10, while the most important bond distances and angles are listed in Table 1. The calculated parameters reflect expected C_2 ($TFcPH_2$) or C_1 (*cis*-$Fc_2Ph_2PH_2$) effective symmetries in the complexes under consideration. In all cases, the global minima require formation of α,β,α,β-($TFcPH_2$) or α,β-(*cis*-$Fc_2Ph_2PH_2$) atropoisomers. As expected, the ferrocene substituents are not coplanar with the porphyrin core with C(α-Porph)–C(*meso*)–C(*ipso*)–C(α-Cp) torsion angles varying between 43.2 and 45.7° (Table 1). The optimized porphyrin core for all complexes under consideration

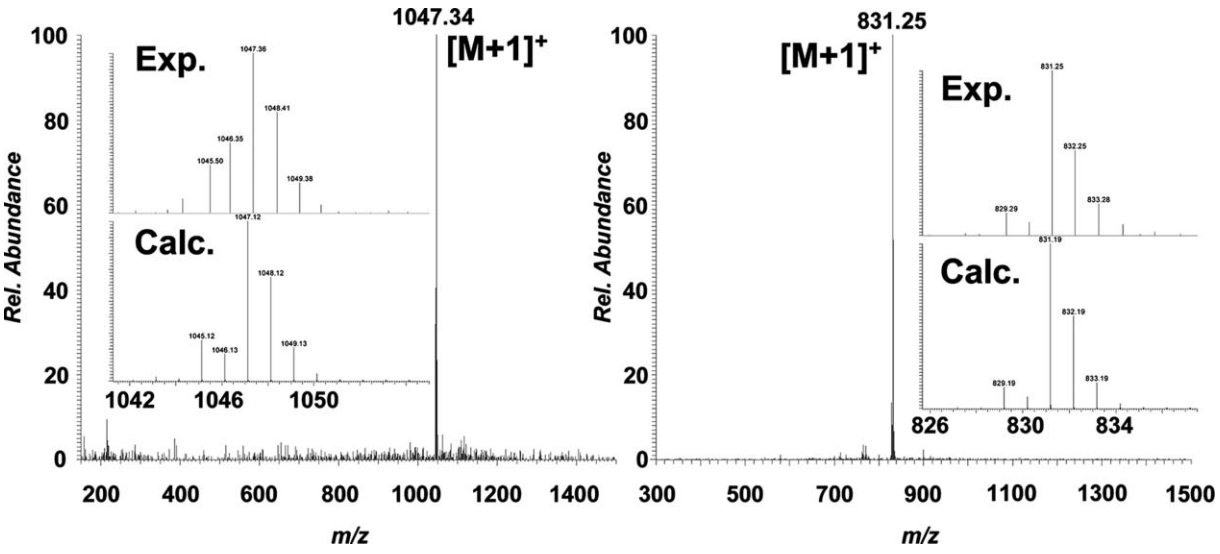

Fig. 7 APCI-MS spectra of $TFcPH_2$ (left) and *cis*-$Fc_2Ph_2PH_2$ (right) in THF.

Table 1 Selected bond distances and torsion angles for optimized structures of $TFcPH_2$ and both NH tautomers of *cis*-$Fc_2Ph_2PH_2$

	$TFcPH_2$	*cis*-$Fc_2Ph_2PH_2$ (**A**)	*cis*-$Fc_2Ph_2PH_2$ (**B**)
Bond distances/Å			
Fe_1–Fe_2	9.763	9.810	9.747
Fe_1–Fe_3	12.043	—	—
Fe_1–Fe_4	9.828	—	—
Fe_2–Fe_3	9.828	—	—
Fe_2–Fe_4	11.981	—	—
Fe_3–Fe_4	9.763	—	—
Torsion angles/°			
C_α–C_{meso}–C_i(cp1)-C_α(cp1)[a]	43.685	45.656	44.937
C_α–C_{meso}–C_i(cp2)-C_α(cp2)	43.198	43.515	43.205
C_α–C_{meso}–C_i(cp3)-C_α(cp3)	43.685	—	—
C_α–C_{meso}–C_i(cp4)-C_α(cp4)	43.198	—	—

[a] cp1–cp4 represents substituted cyclopentadienyl ligands of respective iron centers.

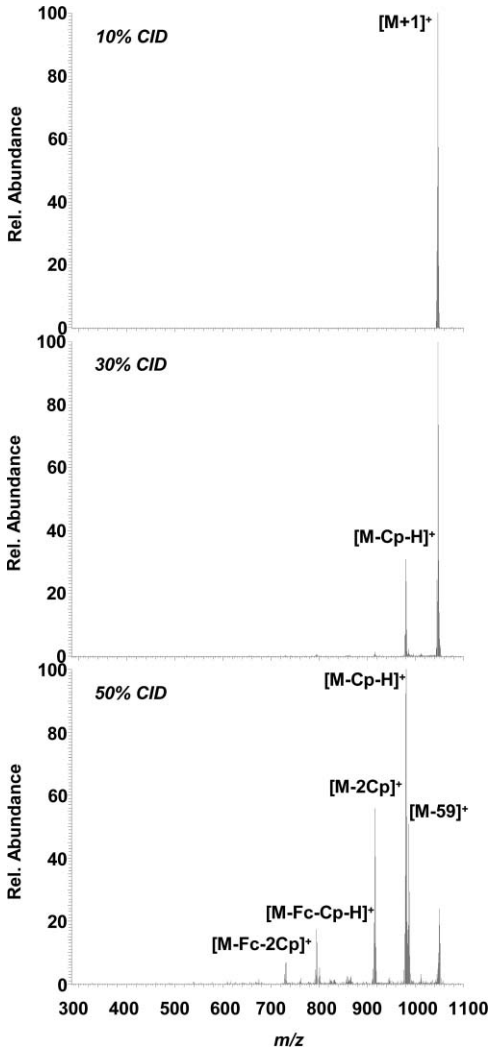

Fig. 8 APCI-MS/MS spectra of $TFcPH_2$ at different collision-induced dissociation energies.

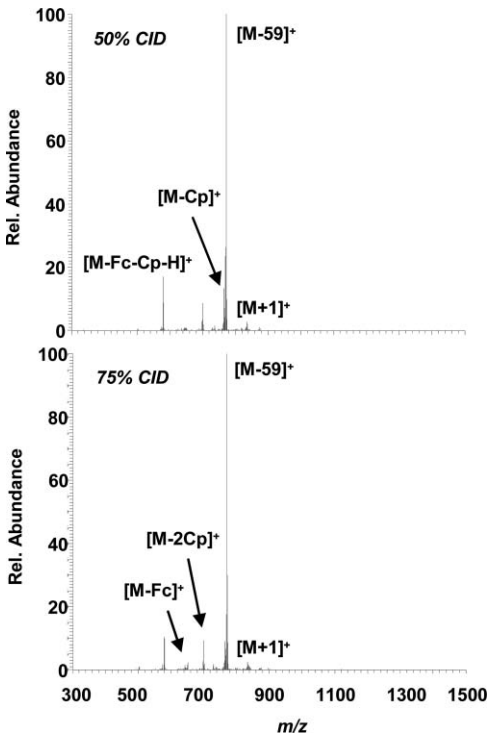

Fig. 9 APCI-MS/MS spectra of *cis*-$Fc_2Ph_2PH_2$ at different collision-induced dissociation energies.

adopts a saddle conformation, with $TFcPH_2$ complex showing slightly larger deviations from the N_4 plane. The molecular orbital diagram for $TFcPH_2$ and both possible tautomers of *cis*-$Fc_2Ph_2PH_2$ is presented in Fig. 11, while frontier molecular orbitals are depicted in Fig. 12. C_2 or C_1 effective symmetries observed in the case of $TFcPH_2$ and *cis*-$Fc_2Ph_2PH_2$, respectively, raise any possible degeneracy from molecular orbitals. In all cases, HOMO predominantly consists of cyclopentadienyl ligands π orbitals coupled with the iron d_{xy} atomic orbital. This orbital is energetically separated from the series of lower-energy, almost pure ferrocenyl-based molecular orbitals (Table 2). As expected, iron d_{xy}, $d_{x^2-y^2}$, and d_{z^2} atomic orbitals contribute to the formation of these ferrocene-based MOs. Again, in all cases, LUMO and LUMO + 1 are almost degenerate and predominantly porphyrin-based π* orbitals energetically well-separated from the LUMO + 2 and higher energy unoccupied MOs, which have significant

Table 2 Molecular orbital compositions of selected orbitals in $TFcPH_2$ and two NH tautomers of *cis*-$Fc_2Ph_2PH_2$ predicted at the DFT level[a]

	$TFcPH_2$			*cis*-$Fc_2Ph_2PH_2$ (**A**)				*cis*-$Fc_2Ph_2PH_2$ (**B**)			
	Composition				Composition				Composition		
E/eV	Fe	Fc	P	*E*/eV	Fe	Fc	P	*E*/eV	Fe	Fc	P
−4.311	80.8	97.6	2.4	−5.912	2.9	38.4	43.6	−5.867	5.0	58.5	37.9
−4.298	81.2	97.8	2.2	−5.625	1.3	7.8	90.0	−5.618	1.3	6.5	91.4
−4.268	74.5	93.4	6.6	−5.537	1.1	5.9	93.0	−5.538	0.7	5.0	93.8
−4.116	59.2	98.3	1.7	−4.955	3.0	7.0	90.0	−4.956	3.2	7.3	89.7
−4.112	59.3	98.4	1.6	−4.655	19.3	36.4	56.3	−4.653	19.6	36.8	56.1
−4.103	57.2	97.5	2.5	−4.498	85.5	97.7	2.2	−4.498	85.8	98.0	2.0
−4.092	58.8	97.7	2.3	−4.464	77.6	90.8	8.4	−4.467	76.8	90.0	9.1
−4.089	58.2	98.0	2.0	−4.230	61.8	97.9	2.1	−4.230	61.8	98.1	1.9
−4.078	56.7	98.0	2.0	−4.214	61.1	97.5	2.5	−4.219	61.5	97.4	2.5
−4.074	56.0	96.8	3.2	−4.197	59.4	97.5	2.4	−4.195	59.3	97.6	2.4
−3.877	**39.0**	**68.4**	**31.6**	**−4.120**	**52.1**	**85.0**	**13.5**	**−4.127**	**51.5**	**84.0**	**14.2**
−2.620	***8.2***	***21.3***	***78.7***	***−2.869***	***6.0***	***14.0***	***78.5***	***−2.874***	***5.2***	***12.6***	***79.1***
−2.591	7.2	19.4	80.6	−2.854	4.3	10.9	81.0	−2.849	5.1	12.5	80.1
−1.668	23.9	49.7	50.3	−1.824	21.5	44.2	48.3	−1.836	22.5	45.9	47.1
−1.228	43.3	94.7	5.3	−1.584	42.1	93.6	6.3	−1.583	42.1	94.1	5.8
−1.222	42.6	94.2	5.8	−1.563	41.9	94.8	5.0	−1.565	42	94.9	4.9
−1.200	43.3	95.4	4.6	−1.515	42.8	95.6	4.1	−1.507	42.1	94.1	5.2
−1.195	43.7	96.7	3.3	−1.314	24.4	58.4	28.2	−1.325	23.7	56.5	28.6

[a] HOMO is labeled in bold and LUMO is labeled in bold italic.

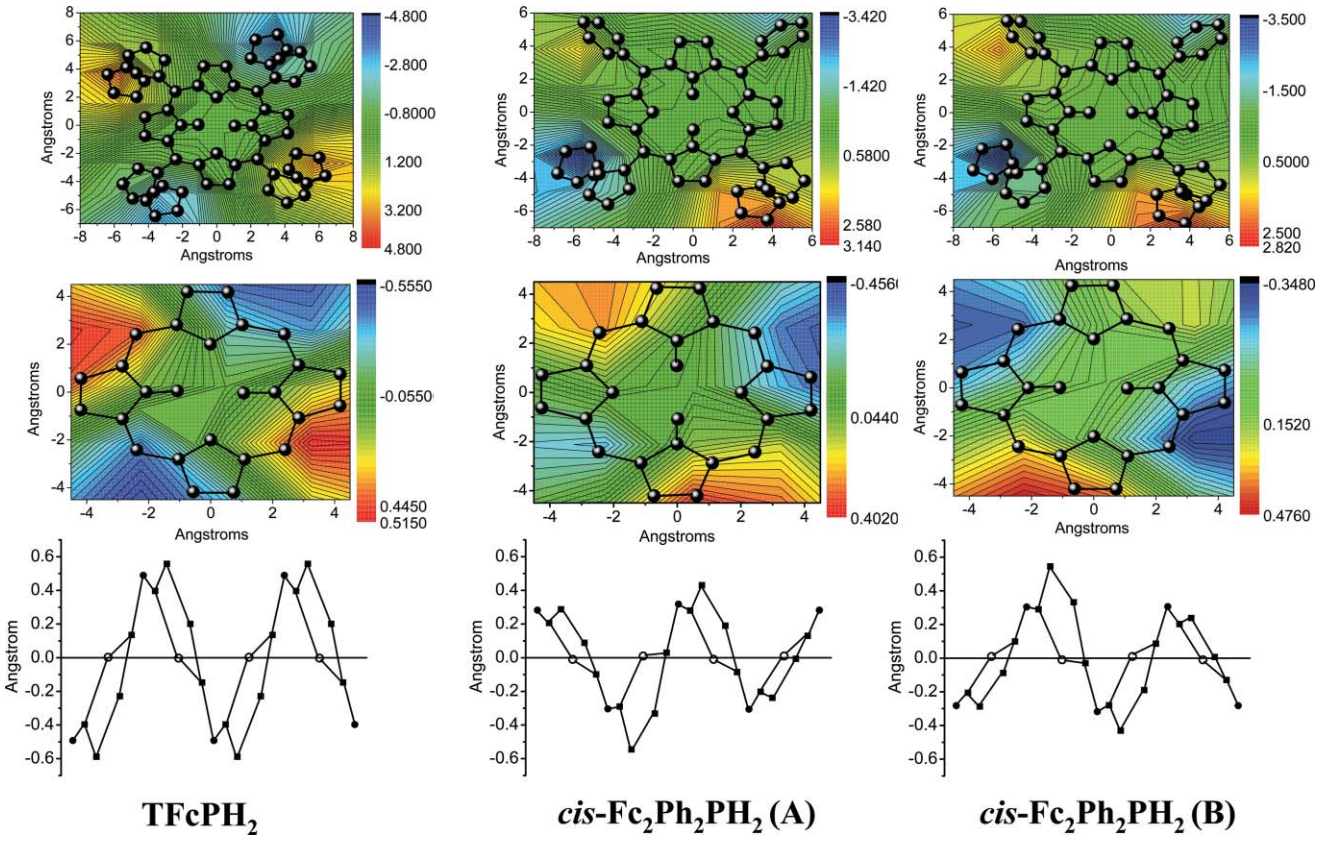

Fig. 10 2D counterplot analyses and linear display deviations from planarity calculated for $TFcPH_2$ and *cis*-$Fc_2Ph_2PH_2$.

contributions from iron d_{xz} and d_{yz} atomic orbitals (Table 2). Validity of the electronic structure of $TFcPH_2$ and *cis*-$Fc_2Ph_2PH_2$ was further supported by calculation of Mössbauer quadrupole splittings in these complexes (Table 3). Indeed, the calculated quadrupole splitting and asymmetry parameter in $TFcPH_2$ are in excellent agreement with the experimental data, while those calculated for *cis*-$Fc_2Ph_2PH_2$ compound are in a range of values that are expected for ferrocenyl-containing compounds.[10,11]

Redox properties of $TFcPH_2$ and *cis*-$Fc_2Ph_2PH_2$ were investigated by cyclic voltammetry (CV) and differential pulse voltammetry (DPV) methods using *o*-dichlorobenzene (*o*-DCB, $\varepsilon = 9.93$) as a solvent. Results are graphically presented in Fig. 13,

Table 3 DFT predicted Electric Field Gradient components and quadrupole splittings for $TFcPH_2$ and two NH tautomers of *cis*-$Fc_2Ph_2PH_2$

Center	V_{xx}/au	V_{yy}/au	V_{zz}/au	ΔE_q/mm s^{-1}
$TFcPH_2$[a]				
Fe_1	0.661	0.801	−1.462	−2.372
Fe_2	0.663	0.795	−1.458	−2.365
Fe_3	0.663	0.795	−1.458	−2.365
Fe_4	0.661	0.801	−1.462	−2.372
cis-$Fc_2Ph_2PH_2$ (**A**)				
Fe_1	0.723	0.856	−1.579	−2.560
Fe_2	0.720	0.855	−1.575	−2.554
cis-$Fc_2Ph_2PH_2$ (**B**)				
Fe_1	0.725	0.852	−1.577	−2.556
Fe_2	0.717	0.860	−1.577	−2.557

[a] Experimental room-temperature quadrupole splitting is 2.37 mm s^{-1}.

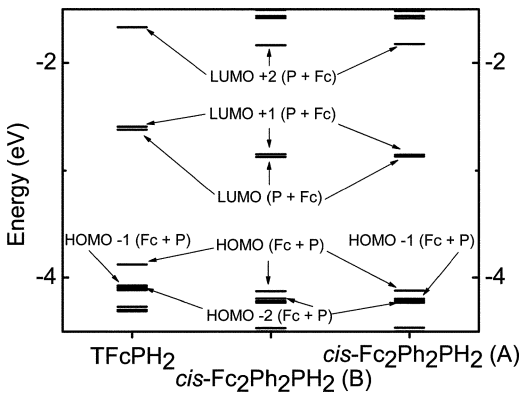

Fig. 11 Molecular orbital diagram of $TFcPH_2$ and both tautomers of *cis*-$Fc_2Ph_2PH_2$ calculated at the DFT level.

and redox potentials are indicated in Table 4. Both complexes undergo two successful reversible one-electron reduction processes

Table 4 Redox potentials (Fc/Fc^+) for $TFcPH_2$ and *cis*-$Fc_2Ph_2PH_2$ complexes in 0.1 M TBAP/*o*-DCB solution

2nd Reduction	1st Reduction	1st Oxidation	2nd Oxidation	3rd Oxidation
$TFcPH_2$				
−2.10	−1.86	−0.10	+0.03	+0.63
***cis*-$Fc_2Ph_2PH_2$**				
−2.05	−1.76	+0.03	+0.12	+0.68

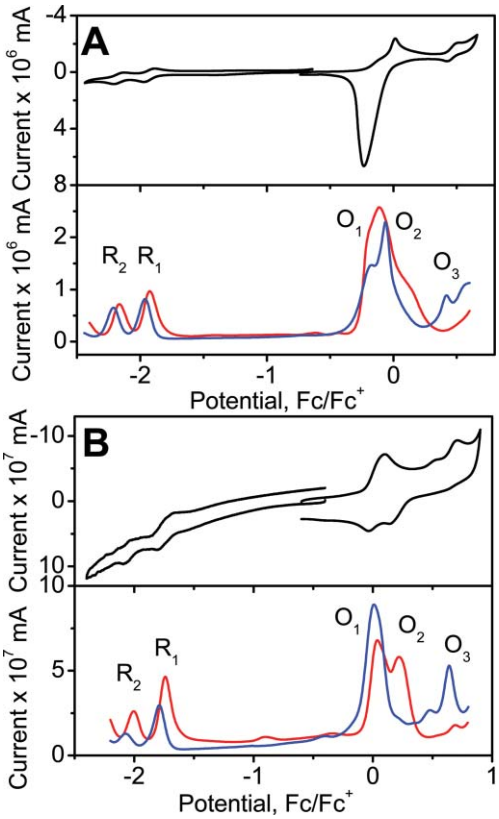

Fig. 13 CV (top) and DPV (bottom) data for $TFcPH_2$ (A) and *cis*-$Fc_2Ph_2PH_2$ (B) in 0.1 M TBAP/*o*-DCB solution.

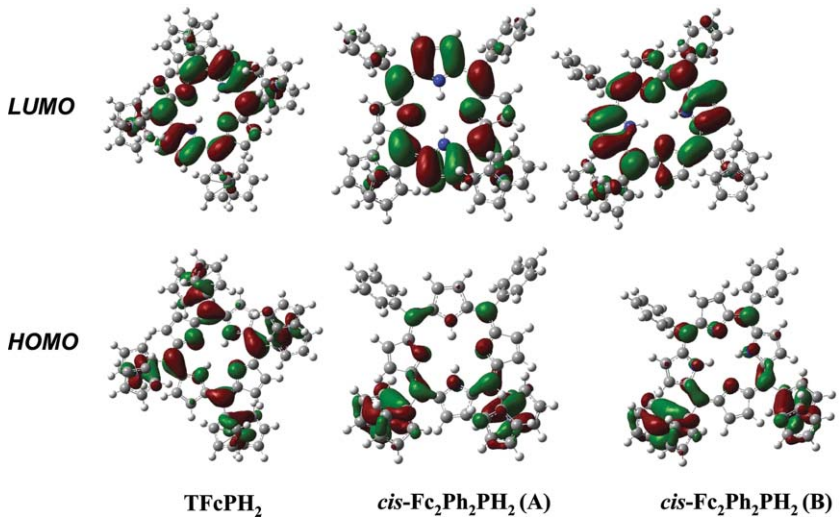

Fig. 12 Frontier orbitals of $TFcPH_2$ and both tautomers of *cis*-$Fc_2Ph_2PH_2$ calculated at the DFT level.

with potentials close to *meso*-tetraarylsubstituted metal-free porphyrins indicating the formation of respective porphyrin anions and dianions.[12] CV and DPV data for $TFcPH_2$ complex reveals three consecutive oxidation processes (Fig. 13). Both CV and DPV experiments indicate that the first two processes are two-electron in nature, while the third is a one-electron oxidation. The first and second anodic oxidation components are closely spaced with the first oxidation wave appearing as a shoulder on the CV curve, which can be resolved using the DPV technique. The cathodic component for the first and second oxidation processes, however, appears as a single sharp peak on the CV curve but has a shoulder in the case of the DPV experiment (Fig. 13). A similar cathodic sharp peak has been observed in numerous polyferrocenyl-containing phthalocyanines and is clearly indicative of an adsorption/desorption process on the electrode.[13]

In general, such behavior indicates the deposition of $[TFcPH_2]^{4+}$ cations (originated as a result of successful consequential "2 + 2" oxidation of ferrocenyl substituents) on the electrode. The one-electron nature of all reduction and third oxidation processes along with the typical value (2.2 V)[12] for porphyrin cation–radical–porphyrin anion–radical pair potential separation between the third oxidation and first reduction potentials allowed us to assign these redox processes as porphyrin-based ones.

On the other hand, the closely separated "2 + 2" first and second oxidation processes can clearly be assigned to four-electron oxidation of all iron(II) to iron(III) centers, which further was confirmed by chemical and electrochemical oxidation experiments. Although the difference between the first and second oxidation processes in $TFcPH_2$ is small (130 mV, $K_c = 157.5$) in comparison to the previously reported mixed-valence porphyrins,[2] it is clear that a mixed-valence state in $TFcPH_2$ can be achieved, at least theoretically, by chemical or electrochemical oxidation of the initially neutral complex. The anodic component for the first and second oxidation processes in *cis*-$Fc_2Ph_2PH_2$, appears as a single sharp peak on CV and DPV curves (Fig. 13). On the other hand, the cathodic peak splits into two components, indicating the stepwise desorption of $[cis\text{-}Fc_2Ph_2PH_2]^+$ and $[cis\text{-}Fc_2Ph_2PH_2]^{2+}$cations (originated as a result of successful consequential "1 + 1" oxidation of ferrocenyl substituents) on the electrode. Again, the one-electron nature of all reductions and the third oxidation processes along with potential separation (2.2 V)[12] between third oxidation and first reduction potentials allowed us to assign these redox processes as porphyrin-based. On the other hand, closely separated "1 + 1" first and second oxidation processes can be clearly assigned to two-electron oxidation of all iron(II) to iron(III) centers, which was further confirmed by chemical and electrochemical oxidation experiments, although the difference between the first and second oxidation processes in *cis*-$Fc_2Ph_2PH_2$ is even smaller (90 mV, $K_c =$ 33.2) in comparison to that in $TFcPH_2$ and previously reported mixed-valence porphyrins.[2]

The observation of successful consecutive oxidations of ferrocene substituents in $TFcPH_2$ and *cis*-$Fc_2Ph_2PH_2$ complexes is in strong disagreement with the earlier proposed hypothesis according to which, the mixed-valence state formation is only possible in conformationally rigid polyferrocenyl-containing porphyrins.[2a] It should be noted that the recent electrochemical studies on the mixed-valence inorganic and organometallic systems (including polyferrocenyl-containing complexes) are clearly indicative of the influence of electrolyte nature and type of solvent on the observed oxidation potentials and oxidation waves splitting.[14,15] Moreover, it was recently shown that it is possible to manipulate one-electron and two-electron oxidation pathways in (fulvalendiyl)dirhodium complexes by simply changing the nature of the electrolyte, and thus, use of only electrochemical data for the description of mixed-valence states was strongly questioned.[14a] For instance, it is was suggested that the use of electrochemical data in calculation of comproportionation constants for mixed-valence compounds, strictly speaking, can lead to erroneous results in the description of the degree of metal–metal coupling, and indeed, use of the inter-valence charge-transfer (IVCT) band position and its intensity was recommended as a better indicator of the extent of inter-metal communication in polynuclear transition-metal complexes.[15] Interestingly, very recently it was shown that the use of the weakly coordinating electrolyte, $\{NBu_4\}\{B(C_6F_5)_4\}$ is responsible for observation of two successful one-electron oxidations of ferrocene substituents in the perfluorophenyl analogue of *cis*-$Fc_2Ph_2PH_2$ complex.[16] Although the authors did not discuss accessibility of the mixed-valence states in these analogue complexes, the first and second oxidation wave splittings (~100 mV) are close to those observed in $TFcPH_2$ and *cis*-$Fc_2Ph_2PH_2$ in *o*-DCB–TBAP system. Thus, in order to confirm the possibility of the formation of mixed-valence states in $TFcPH_2$ and *cis*-$Fc_2Ph_2PH_2$, we compared their spectroscopic changes under chemical and spectroelectrochemical oxidation conditions.

Chemical oxidation of $TFcPH_2$ and *cis*-$Fc_2Ph_2PH_2$ by tetracyanoethylene (TCE) leads to similar changes in the UV-Vis spectra (Fig. 2). Thus, in the case of $TFcPH_2$, the Soret band shifts from 433 to 457 nm, Q-bands at 664 and 728 nm disappear, and two new bands at 599 and 909 nm appear in the UV-Vis spectrum. The spectral changes were further confirmed by MCD spectroscopy, according to which the Soret band represented by a Faraday pseudo *A*-term centered at 435 nm transforms upon oxidation into a Faraday pseudo *A*-term centered at 457 nm, the initial Faraday *B*-terms at 669 and 727 nm disappear, and a new Faraday *B*-term at 593 nm and pseudo *A*-term centered at 921 nm appear in the spectrum (Fig. 2). Interestingly, the energy of the last band is close to that observed in the mixed-valence state of metal-free octa-β-alkyl-5,-15-bisferrocenylporphyrin,[2a] and thus, it was first tentatively assigned as an IVCT band. Further support of this assignment and evidence pointing to the formation of a mixed-valence state in $TFcPH_2$ was obtained on the basis of Mössbauer spectroscopy and spectroelectrochemical experiments. The initial Mössbauer spectrum of $TFcPH_2$ consists of one doublet with parameters typical for low-spin iron(II) ferrocene-containing compounds ($\delta_{Fe} = 0.45$ mm s^{-1}, $\Delta E_Q = 2.37$ mm s^{-1}, 295 K). This single doublet changes upon chemical oxidation with TCE into two doublets with one corresponding to low-spin iron(II) ferrocene ($\delta_{Fe} = 0.45$ mm s^{-1}, $\Delta E_Q = 2.24$ mm s^{-1}, 295 K) and the other to low-spin iron(III) ferricinium-type parameters ($\delta_{Fe} =$ 0.12 mm s^{-1}, $\Delta E_Q = 0.54$ mm s^{-1}, 295 K). The relative ratio for these two doublets, in general, depends on the amount of oxidant used (TCE) but become a constant (1 : 1) when large excess (4 to 100 molar excess) of TCE is used for the oxidation. This is clearly indicative of an oxidation of only two out of four possible iron centers and the formation of mixed-valence $[TFcPH_2]^{2+}$.[6] The observed Mössbauer spectrum of $[TFcPH_2]^{2+}$ is clearly indicative of the so-called trapped valence situation in this mixed-valence

complex. Thus, it has been shown that Mössbauer spectroscopy can be used to monitor the intramolecular electron-transfer rate in mixed-valence systems.[17] In fact, when the electron-transfer rate is slower than *ca.* 10^7 s^{-1}, then the Mössbauer spectrum should consist of a superposition of two quadrupole-splitted doublets with characteristics typical for iron(II) and iron(III) metallocenes.[17] Next, as it was discussed earlier for the large number of bisferrocenyl-containing compounds, with prominent metal–metal coupling, the quadrupole splittings of the ferrocene site in the one-electron oxidized species are smaller in comparison to those in the starting materials because of the electron density donation from the non-oxidized ferrocene site to the oxidized ferricinium moiety.[17] The Mössbauer spectra of $TFcPH_2$ under TCE titration experiments are in the excellent agreement with the above mentioned observation. Indeed, the quadrupole splitting for the ferrocene-containing sites in $TFcPH_2$ oxidized by TCE are significantly reduced from 2.36 to 2.24 mm s^{-1}.

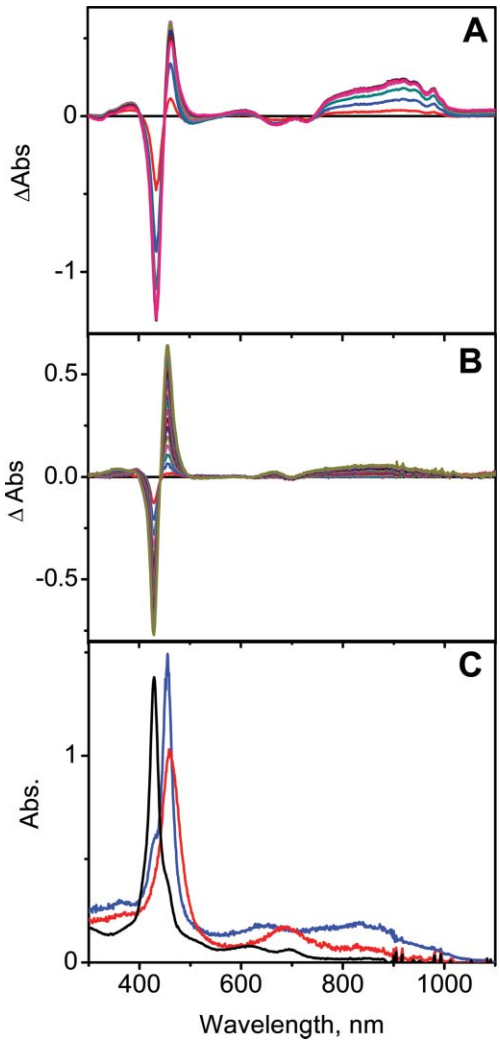

Fig. 14 Differential UV-Vis spectra under spectroelectrochemical transformation of $TFcPH_2$ into $[TFcPH_2]^{2+}$ (A) and *cis*-$Fc_2Ph_2PH_2$ into $[cis\text{-}Fc_2Ph_2PH_2]^+$ (B). Individual scans were taken every 10 min. UV-Vis spectra of *cis*-$Fc_2Ph_2PH_2$ (black), $[cis\text{-}\ Fc_2Ph_2PH_2]^+$ (blue), and $[cis\text{-}Fc_2Ph_2PH_2]^{2+}$ (red) (C).

Spectroelectrochemical oxidation of $TFcPH_2$ at the first oxidation potential is consistent with changes observed in the UV-Vis spectrum of $TFcPH_2$ during chemical oxidation again supporting the assignment of the near-IR band as IVCT (Fig. 14). Although one can assume that the electrochemically observed small difference in the first and second oxidation potentials in $TFcPH_2$ should not allow the formation of pure $[TFcPH_2]^{2+}$, we were able to observe a partial transformation of the starting $TFcPH_2$ into $[TFcPH_2]^{2+}$ with pure isobestic points in the UV-Vis spectrum when electrolysis was conducted at a slightly lower potential in comparison to that indicated in Table 4. On the other hand, when UV-Vis spectra were taken on the solution of $[TFcPH_2]^{2+}$ at the first oxidation potential mentioned in Table 4, no clear isobestic points were observed because of the presence of both $[TFcPH_2]^{2+}$ and $[TFcPH_2]^{4+}$ cations in solution. All attempts to conduct electrolysis of $[TFcPH_2]^{2+}$ at the second oxidation potential (second two-electron oxidation wave) resulted in slow deposition of $[TFcPH_2]^{4+}$ on the electrodes and an overall decay of optical density. The second oxidation process, however, is reversible under spectroelectrochemical conditions as was seen from the re-appearance of $TFcPH_2$ during electrolytic reduction of precipitated $[TFcPH_2]^{4+}$. Similar results were obtained for *cis*-$Fc_2Ph_2PH_2$. Indeed, when monitored by UV-Vis spectroscopy, chemical oxidation of *cis*-$Fc_2Ph_2PH_2$ leads to a red shift of the Soret band from 426 to 452 nm (both represented by Faraday pseudo *A*-terms in MCD), disappearance of Q-bands at 616 and 692 nm, and appearance of bands at 610 (resulted in Faraday *B*-term in MCD) and 803 nm (appeared as Faraday pseudo *A*-term in MCD) with the last band assigned as IVCT (Fig. 2). Since *cis*-$Fc_2Ph_2PH_2$ has only two ferrocenyl substituents, it is logical to expect that the dication, $[cis\text{-}Fc_2Ph_2PH_2]^{2+}$ will still be soluble under spectroelectrochemical conditions, and thus, provides an opportunity to confirm the disappearance of mixed-valence state upon oxidation of both ferrocenyl substituents. The bulk electrolysis of *cis*-$Fc_2Ph_2PH_2$ at a slightly lower potential than the first oxidation potential indicated in Table 4 resulted in similar changes as were observed during chemical oxidation of *cis*-$Fc_2Ph_2PH_2$ in agreement with the formation of a mixed-valence state $[cis\text{-}Fc_2Ph_2PH_2]^+$ (Fig. 14). Further electrochemical oxidation at a slightly higher potential than the second oxidation potential indicated in Table 4 leads to a decrease in intensity and a slight red-shift of the Soret band, a disappearance of the IVCT band and the band located at 610 nm, and an appearance of a new band located at 690 nm (Fig. 14). The disappearance of the IVCT band clearly supports the formation of $[cis\text{-}Fc_2Ph_2PH_2]^{2+}$ bis(ferricinium) complex, and thus, provides additional evidence for the presence of the initial mixed-valence state in $[cis\text{-}Fc_2Ph_2PH_2]^+$.

Unlike that proposed by Burrrell *et al.*,[2a] the observation of mixed-valence states in $[TFcPH_2]^{2+}$ and $[cis\text{-}Fc_2Ph_2PH_2]^+$ clearly suggests that the conformational rigidity cannot be considered as the only factor controlling the formation of mixed-valence states in polyferrocenyl porphyrins, although it can, probably, affect the degree of localization/delocalization in these systems. Indeed, the observed difference between the first and second oxidation waves in metal-free octa-β-alkyl-5,-15-bisferrocenylporphyrin (~190 mV) is significantly larger in comparison to that observed in $TFcPH_2$ and *cis*-$Fc_2Ph_2PH_2$. The observation of mixed-valence state formation in *cis*-$Fc_2Ph_2PH_2$ and its absence in

5,15-diferrocenyl-10,20-di-*p*-tolylporphyrin[2a] suggests that the presence of two ferrocenyl substituents in the 5- and 10-positions of the porphyrin core might be one of the necessary conditions for the formation of long-range metal–metal coupling in conformationally flexible polyferrocenyl-containing porphyrins. Indeed, our DFT calculations on the zinc complex of $[TFcPH_2]^{2+}$ support an oxidation of two iron atoms at the 5- and 10-positions of the porphyrin core as can be seen from the increase of spin density and decrease of electric field gradient on these centers, while all of our attempts to optimize the molecular structure of $[TFcPH_2]^{2+}$ with iron(III) centers at 5- and 15-positions have failed (ESI†). Of course, DFT calculations cannot be considered as the definitive proof of charge localization in $[TFcPH_2]^{2+}$, but they may serve as a starting point for the understanding of redox properties in $TFcPH_2$ and *cis*-$Fc_2Ph_2PH_2$. We speculate that the differences in mixed-valence state formation in $TFcPH_2$, *cis*-$Fc_2Ph_2PH_2$, and 5,15-diferrocenyl-10,20-di-*p*-tolylporphyrin can be explained by the differences in effective metal–metal distances in these compounds. These distances were estimated to be between 8 and 10 Å for ferrocenyl substituents at 5- and 10-positions, while they lie between 12 and 13 Å in the case of substituents at 5- and 15-positions. Our explanation is in accordance with the previously observed distance-dependable mixed-valence state formation in numerous bis(ferrocenyl)-containing systems linked *via* unsaturated substituents.[18] Although such a distance dependable treatment of the formation of the mixed-valence states in $TFcPH_2$ and *cis*-$Fc_2Ph_2PH_2$ looks reasonable, it should be considered with caution in sight of the very recent electrochemical data published on perfluorophenyl analogues of *cis*- and *trans*-$Fc_2Ph_2PH_2$ according to which the difference between the first and second oxidation potentials in *cis*-(5,10-disubstituted) and *trans*-(5,15-disubstituted) isomers is virtually the same.[16] Indeed, our[3b] and recently published[16] data on redox properties of conformationally flexible ferrocene-containing porphyrins leads to the fundamental question: does chemical or electrochemical (in non-polar solvent/weakly coordinating electrolyte solution) oxidation of 5,15-diferrocenyl-10,20-di-*p*-tolylporphyrin generate a mixed-valence state in this compound?

Finally, as it was recently discussed in the literature,[14,15] instead of the use of electrochemical data, the position, half-width and intensity of the intense IVCT band in $[TFcPH_2]^{2+}$ and [*cis*-$Fc_2Ph_2PH_2]^+$ could be used as a marker, allowing a description of the degree of metal–metal coupling in these systems. This can be calculated on the basis of the procedure previously published in literature.[1,7] Taking into consideration conformational flexibility of ferrocenyl substituents in $[TFcPH_2]^{2+}$ and [*cis*-$Fc_2Ph_2PH_2]^+$, the electronic coupling term, H_{ab}, has been estimated in the ranges of 1747–2183 and 1106–1382 cm^{-1}, respectively, which puts both systems within Class II mixed-valence complexes in the Robin and Day classification,[1a,1b] in agreement with the Mössbauer data available for $[TFcPH_2]^{2+}$. The comparable values of H_{ab} and λ, however, do not allow us to specifically describe the compounds $[TFcPH_2]^{2+}$ and [*cis*-$Fc_2Ph_2PH_2]^+$ as weakly-coupled or strongly-coupled Class II mixed-valence complexes.

Conclusions

In summary, metal-free 5,10,15,20-tetraferrocenylporphyrin and 5,10-bisferrocenyl-15,20-bisphenylporphyrin have been prepared and characterized by UV-Vis, MCD, ^1H, ^{13}C, and variable-temperature NMR, APCI- and ESI-MS, and Mössbauer spectroscopy, while their redox properties were investigated using electrochemical (cyclic voltammetry and differential pulse voltammetry), spectroelectrochemical, and chemical oxidation approaches. The electronic structure calculations at the Density Functional Theory level reveal that both compounds adopt a saddle conformation and the HOMOs in both complexes are predominantly metal-centered, while the LUMOs predominantly consist of porphyrin π^* orbitals. In spite of the rotational freedom of ferrocenyl substituents, both metal-free 5,10,15,20-tetraferrocenylporphyrin and 5,10-bisferrocenyl-15,20-bisphenylporphyrin are able to form mixed-valence states upon the successive ferrocene-based two- and one-electron oxidations, respectively, as confirmed by UV-Vis, MCD, Mössbauer, electro-, and spectroelectrochemical methods and thus, the earlier suggested (Boyd *et al. Chem. Commun.*, 1999, 637) requirements for the formation of mixed-valence states in ferrocene-containing porphyrins should be revised.

Experimental

General methods

All reactions were performed under a dry nitrogen atmosphere with flame-dried glassware. Pyrrole, ferrocenecarbaldehyde, benzaldehyde, boron trifluoride etherate, and chloranil, and triethylamine were purchased from commercially available sources and used without further purification. Silica gel (60 Å, 32–63 mesh) was purchased from Sorbent Technologies, basic aluminium oxide (Activity I, 58 Å, 150 mesh) was purchased from Fischer Inc., Bio-Beads (SX-1 and SX-3) for size exclusion filtration were purchased from Bio-Rad. For electrochemical experiments, anhydrous *o*-dichlorobenzene was used without further purification, while tetrabutyl ammonium perchlorate (TBAP) was recrystallized from ethyl acetate. NMR spectra were recorded on Varian INOVA instrument with 500 MHz frequency for protons and 125 MHz for carbon. Chemical shifts are reported in ppm and referenced to TMS as an internal standard. UV-Vis data were obtained on HP 8453 or Cary 17 spectrometers. MCD data were recorded using an OLIS DCM 17 CD spectropolarimeter using a 1.4 T DeSa magnet. Electrochemical measurements were conducted using a CH electrochemical analyzer utilizing a three-electrode scheme with platinum electrodes and a 0.1 M solution of TBAP in *o*-dichlorobenzene. Potentials were corrected using an internal standard (ferrocene) in all cases. Spectroelectrochemical data were collected in a 0.3 M solution of TBAP in DCB at −0.13 (1st oxidation) and +0.07 V (2nd oxidation) for $TFcPH_2$ and +0.01 (1st oxidation) and +0.14 V (2nd oxidation) for *cis*-$Fc_2Ph_2PH_2$. APCI-MS, APCI-MS/MS, and LC-MS experiments were conducted using a Finnegan LCQ LC-MS system. High-resolution mass spectra were obtained using a Bruker HR-MS instrument.

Computational details

All DFT calculations were conducted using *Gaussian 03* software package[19] running under either Windows or UNIX OS. Geometries were obtained *via* optimization with Becke's exchange functional[20] and Perdew non-local correlation functional[21] (BP86)

coupled with Wachter's full-electron basis set for the iron atom and 6-31G(d)[22] basis set for all other atoms. For all optimized structures, frequency calculations were carried out to ensure optimized geometries represented local minima. In the case of single point calculations, Becke's pure exchange functional and Perdew and Wang's correlation functional[23] (BPW91) were used. Wachter's original full-electron basis set[24] (contracted as 62111111/3311111/3111) with one set of polarization functions was used for the iron atom, while for all other atoms 6-311G(d) basis set was employed. Mössbauer quadrupole splittings (ΔE_Q) and asymmetry parameters (η) were calculated using DFT predicted principle components of the electric field gradient tensor (V_{ii}) at the ^{57}Fe nucleus as discussed earlier.[11]

Synthesis

5,10,15,20-tetraferrocenylporphyrin. A mixture of 1.2 g (0.0056 mol) of ferrocenecarbaldehyde, 0.4 g (0.006 mol) pyrrole, and 0.038 ml (0.0003 mol) $BF_3{\cdot}Et_2O$ in CH_2Cl_2 (150 ml) was reacted for 20 h at room temperature in argon atmosphere. After this period, 0.98 g (0.004 mol) of chloranil was added and the resulting mixture was refluxed for 3.5 h. After solvent evaporation, the residue was chromatographed on silica gel using a toluene–triethylamine mixture (100 : 1 v/v) as the eluent. Finally, the product was recrystallized from toluene–hexane. Yield 0.587 g (40%). Selected spectroscopic data: UV-VIS (λ_{max}/nm, $CHCl_3$, $\varepsilon \times 10^{-4}$): 233 (12.7), 664 (1.43), 728 (1.27); mixed-valence dication: 457 (15.16), 607 (1.18), 909 (3.31). ^{1}H-NMR ($CDCl_3$, TMS, δ): 9.61 (s, 8H, β-pyrr), 5.32 (m, 8H, α-Cp), 4.75 (m, 8H, β-Cp), 3.97 (s, 20H, CpH), −0.49 (s, 2H, NH). ^{13}C-NMR ($CDCl_3$, TMS, δ): 145.9 (α-pyrr), 131.0 (β-pyrr), 117.5 (*meso*-C), 89.4 (C_i–Cp), 77.1 (α-Cp), 70.5 (CpH), 69.2 (β-Cp). MS (APCI, THF, m/z): 1047.13 (100%) $[M + H]^+$. HRMS (ESI, THF, m/z): 1047.1193, Calc. for $C_{60}H_{47}N_4Fe_4$: 1047.1200. Calc. for $C_{60}H_{46}N_4Fe_4$: C, 68.83; H, 4.40; N, 5.35%. Found: C, 68.74; H, 4.48; N, 4.81%.

5,10-bisferrocenyl-15,20-bisphenylporphyrin. A mixture of 0.6 g (0.0028 mol) of ferrocenecarbaldehyde, 0.3 g (0.0028 mol) of benzaldehyde, 0.4 g (0.006 mol) pyrrole, and 0.038 ml (0.0003 mol) $BF_3{\cdot}Et_2O$ in CH_2Cl_2 (150 ml) was reacted for 20 h at room temperature in an argon atmosphere. After this period, 0.98 g (0.004 mol) of chloranil was added and the resulting mixture was refluxed for 3.5 h. After solvent evaporation, the residue was chromatographed first on activity I alumina, second and third fractions were collected and further purified sequentially on size-exclusion SX-1 and SX-3 columns and then on several preparative silica gel TLC plates using toluene–triethylamine mixture (98 : 2 v/v) as eluent. Finally, the product was recrystallized from toluene–hexane. Yield 14 mg (1.2%). Selected spectroscopic data: UV-VIS (λ_{max}/nm, $CHCl_3$, $\varepsilon \times 10^{-4}$): 426 (14.01), 616 (0.8), 692 (0.64), $[cis\text{-}Fc_2Ph_2PH_2]^+$ 360 (1.58), 452 (14.62), 803 (1.46). ^{1}H-NMR ($CDCl_3$, TMS, δ): 9.90 (s, 2H, β-pyrr-Cp–Cp), 9.78 (d, J = 5 Hz, 2H, β-pyrr-Ph–*Cp*), 8.71 (d, J = 5 Hz, 2H, β-pyrr-*Ph*–Cp), 8.65 (s, 2H, β-pyrr-Ph–Ph), 8.15 (d, J = 6 Hz, 4H, α-Ph), 7.72 (t, J = 6 Hz, 6H, β-Ph + γ-Ph), 5.45 (s, 4H, α-Pc), 4.76 (s, 4H, β-Cp), 4.06 (s, 10H, CpH), −1.83 (s, 2H, NH). ^{13}C-NMR ($CDCl_3$, TMS, δ): 156.7 (α-pyrr-Cp–Cp, vbr), 143.9 (β-pyrr-Ph–Ph, vbr), 141.0 (C_i–Ph), 133.4 ($C_{2,6}$–Ph), 130.2 (β-pyrr-Cp–Cp), 129.6 (β-pyrr-*Cp*–Ph), 129.5 (β-pyrr-Cp–*Ph*), 128.9 (β-pyrr-Ph–Ph), 126.6 (C_4–Ph), 125.7 ($C_{3,5}$–Ph), 118.7 (*meso*-C–Cp), 117.1 (*meso*-C–Ph), 88.6 (C_i–Cp), 76.5 (α-Cp), 69.5 (CpH), 68.0 (β-Cp). MS (APCI, THF, m/z): 831.25 (100%) [M + H]. HRMS (ESI, THF, m/z): 831.1867, Calc. for $C_{52}H_{39}N_4Fe_2$: 831.1871.

Acknowledgements

Generous support from the Research Corporation (Cottrell College Science Award CC6766), University of Minnesota Grant-in-Aid (Grant 20209) and Minnesota Supercomputing Institute to VN as well as University of Minnesota Duluth Undergraduate Research Opportunity Grants to CB and RH is greatly appreciated. We also wish to acknowledge Dr N. M. Loim for the preliminary discussion and synthetic details for the preparation of $TFcPH_2$ and Dr N. Kobayashi for the possibility to collect preliminary electrochemical and MCD data on $TFcPH_2$.

References

1 (*a*) J. S. Miller and A. J. Epstein, *Angew. Chem., Int. Ed. Engl.*, 1994, **33**, 385; (*b*) S. Barlow and D. O'Hare, *Chem. Rev.*, 1997, **97**, 637; (*c*) J.-P. Launay, *Chem. Soc. Rev.*, 2001, **30**, 386; (*d*) A. J. Distefano, J. F. Wishart and S. S. Isied, *Coord. Chem. Rev.*, 2005, **249**, 507; (*e*) K. D. Demadis, C. M. Hartshorn and T. J. Meyer, *Chem. Rev.*, 2001, **101**, 2655.
2 (*a*) P. D. W. Boyd, A. K. Burrell, W. M. Campbell, P. A. Cocks, K. C. Gordon, G. B. Jameson, D. L. Officer and Z. Zao, *Chem. Commun.*, 1999, 637; (*b*) S. W. Rhee, Y. H. Na, T. Do and J. Kim, *Inorg. Chim. Acta*, 2000, **309**, 49.
3 (*a*) N. M. Loim, N. V. Abramova and V. I. Sokolov, *Mendeleev Commun.*, 1996, 46; (*b*) V. N. Nemykin, M. McGinn, A. Y. Koposov, I. N. Tretyakova, E. V. Polshin, N. M. Loim and N. V. Abramova, *Ukr. Chem. J.*, 2005, **71**, 79.
4 (*a*) J. Cheek and J. H. Dawson, in *Porphyrin Handbook*, ed. K. M. Kadish, K. M. Smith and R. Guilard, Academic Press, San Diego, CA, USA, 2000, vol. 7, pp. 339–369; (*b*) J. Mack and M. J. Stilman, in *Porphyrin Handbook*, ed. K. M. Kadish, K. M. Smith and R. Guilard, Academic Press, San Diego, CA, USA, 2003, vol. 16, pp. 43–116.
5 (*a*) H. Friebolin, *Basic one- and two-dimensional NMR spectroscopy*, Wiley-VCH, New York, 4th edn, 2005, pp. 305–334; (*b*) J. I. Kaplan and G. Fraenkel, *NMR of chemically exchanging systems*, Academic Press, San Diego, CA, USA, 1980, pp. 71–129.
6 (*a*) H. García-Ortega, J. Crusats, M. Feliz and J. M. Ribó, *J. Org. Chem.*, 2002, **67**, 4170; (*b*) M. J. Crossley, L. D. Field, M. M. Harding and S. J. Sternhell, *J. Am. Chem. Soc.*, 1987, **109**, 2335; (*c*) M. J. Crossley, M. M. Harding and S. J. Sternhell, *J. Am. Chem. Soc.*, 1986, **108**, 3608.
7 (*a*) J. Hennig and H.-H. Limbach, *J. Chem. Soc., Faraday Trans. 2*, 1979, **75**, 752; (*b*) S. S. Eaton and G. R. Eaton, *J. Am. Chem. Soc.*, 1977, **99**, 1601.
8 (*a*) V. N. Nemykin and P. Basu, *Inorg. Chim. Acta*, 2005, **358**, 2876; (*b*) V. N. Nemykin and P. Basu, *Dalton Trans.*, 2004, 1928; (*c*) C. P. G. Butcher, P. J. Dyson, B. F. G. Johnson, T. Khimyak and J. S. McIndoe, *Chem.–Eur. J.*, 2003, **9**, 944; (*d*) E. Crawford, P. J. Dyson, O. Forest, S. Kwok and J. S. McIndoe, *J. Cluster Sci.*, 2006, **17**, 47.
9 (*a*) G. J. Van Berkel, S. A. McLuckey and G. L. Glish, *Anal. Chem.*, 1991, **63**, 1098; (*b*) M. R. M. Domingues, M. G. O. S.-Marques, P. Domingues, M. G. Neves, J. A. S. Cavaleiro, A. J. Ferrer-Correia, O. V. Nemirovskiy and M. L. Gross, *J. Am. Soc. Mass Spectrom.*, 2001, **12**, 381; (*c*) K. S. F. Lau, M. Sadilek, M. Gouterman, G. E. Khalil and C. Brückner, *J. Am. Soc. Mass Spectrom.*, 2006, **17**, 1306; (*d*) V. V. Serra, M. R. M. Domingues, M. A. F. Faustino, P. Domingues, J. P. C. Tomé, M. G. P. M. S. Neves, A. C. Tomé, J. A. S. Cavaleiro and A. J. Ferrer-Correia, *Rapid Commun. Mass Spectrom.*, 2005, **19**, 2569.
10 E. Fluck, in *Chemical Applications of Mössbauer spectroscopy*, ed. V. I. Goldanskii and R. H. Herber, Academic Press Inc., New York, 1968, pp. 268.
11 V. N. Nemykin and R. G. Hadt, *Inorg. Chem.*, 2006, **45**, 8297.
12 K. M. Kadish, E. Van Caemelbecke and G. Royal, in *Porphyrin Handbook*, ed. K. M. Kadish, K. M. Smith and R. Guilard, Academic Press, San Diego, CA, USA, 2000, vol. 9, pp. 1–114.

13 (*a*) Z. Jin, K. Nolan, C. R. McArthur, A. B. P. Lever and C. C. Leznoff, *J. Organomet. Chem.*, 1994, **468**, 205; (*b*) M. J. Cook, G. Cooke and A. Jafari-Fini, *J. Chem. Soc., Chem. Commun.*, 1995, 1715; (*c*) S. Dabak and O. Bekaroglu, *New J. Chem.*, 1997, **21**, 267; (*d*) J. Silver, J. L. Sanchez and C. S. Frampton, *Inorg. Chem.*, 1998, **37**, 411; (*e*) A. Gonzalez, P. Vazquez and T. Torres, *Tetrahedron Lett.*, 1999, **40**, 3263; (*f*) K.-W. Poon, Y. Yan, X. Li and D. K. P. Ng, *Organometallics*, 1999, **18**, 3528.
14 (*a*) F. Barrière and W. E. Geiger, *J. Am. Chem. Soc.*, 2006, **128**, 3980; (*b*) A. Nafady, T. T. Chin and W. E. Geiger, *Organometallics*, 2006, **25**, 1654; (*c*) F. Barrière, R. U. Kirss and W. E. Geiger, *Organometallics*, 2005, **24**, 48.
15 D. M. D'Alessandro and F. R. Keene, *Dalton Trans.*, 2004, 3950.
16 A. Auger and J. C. Swarts, *Organometallics*, 2007, **26**, 102.
17 (*a*) P. Gütlich and J. Ensling, in *Inorganic Electronic Structure and Spectroscopy*, ed. E. I. Solomon and A. B. P. Lever, John Wiley & sons, New York, 1999, vol. 1, pp. 161–211; (*b*) S. Barlow and D. O'Hare, *Chem. Rev.*, 1997, **97**, 637.
18 (*a*) A.-C. Ribou, J.-P. Launay, M. L. Sachtleben, H. Li and C. W. Spangler, *Inorg. Chem.*, 1996, **35**, 3735; (*b*) C. Patoux, C. Coudret, J.-P. Launay, C. Joachim and A. Gourdo, *Inorg. Chem.*, 1997, **36**, 5037; (*c*) Y. J. Chen, D.-S. Pan, C.-F. Chiu, J.-X. Su, S. J. Lin and K. S. Kwan, *Inorg. Chem.*, 2000, **39**, 953.
19 M. J. Frisch, G. W. Trucks, H. B. Schlegel, G. E. Scuseria, M. A. Robb, J. R. Cheeseman, J. A. Montgomery, Jr., T. Vreven, K. N. Kudin, J. C. Burant, J. M. Milam, S. S. Iyengar, J. Tomasi, V. Barone, B. Mennucci, M. Cossi, G. Scalmani, N. Rega, G. A. Petersson, H. Nakatsuji, M. Hada, M. Ehara, K. Toyota, R. Fukuda, J. Hasegawa, M. Ishida, T. Nakajima, Y. Honda, O. Kitao, H. Nakai, M. Klene, X. Li, J. E. Knox, H. P. Hratchian, J. B. Cross, C. Adamo, J. Jaramillo, R. Gomperts, R. E. Stratmann, O. Yazyev, A. J. Austin, R. Cammi, C. Pomelli, J. W. Ochterski, P. Y. Ayala, K. Morokuma, G. A. Voth, P. Salvador, J. J. Dannenberg, V. G. Zakrzewski, S. Dapprich, A. D. Daniels, M. C. Strain, O. Farkas, D. K. Malick, A. D. Rabuck, K. Raghavachari, J. B. Foresman, J. V. Ortiz, Q. Cui, A. G. Baboul, S. Clifford, J. Cioslowski, B. B. Stefanov, G. Liu, A. Liashenko, P. Piskorz, I. Komaromi, R. L. Martin, D. J. Fox, T. Keith, M. A. Al-Laham, C. Y. Peng, A. Nanayakkara, M. Challacombe, P. M. W. Gill, B. Johnson, W. Chen, M. W. Wong, C. Gonzalez and J. A. Pople, *Gaussian 03, Revision C.02*, Gaussian, Inc., Wallingford, CT, 2004.
20 A. D. Becke, *Phys. Rev. A*, 1988, **38**, 3098.
21 C. Lee, W. Yang and R. G. Parr, *Phys. Rev. B*, 1988, **37**, 785.
22 A. D. McLean and G. S. Chandler, *J. Chem. Phys.*, 1980, **72**, 5639.
23 J. P. Perdew and Y. Wang, *Phys. Rev. B*, 1992, **45**, 13244.
24 A. J. H. J. Wachters, *Chem. Phys.*, 1970, **52**, 1033.